Current Biology

An environmentally induced multicellular life cycle of a unicellular cyanobacterium

Highlights

- A unicellular cyanobacterium with a facultative multicellular life cycle

- The phenotypic changes in morphology depend on salinity and population density

- Phenotypic switch is likely mediated by compounds in the medium in a nonlinear way

- Filament fragmentation happens via connection cleavage and not via cell death

Authors

Si Tang, Yuriy Pichugin, Katrin Hammerschmidt

Correspondence

pichugin@princeton.edu (Y.P.),
katrinhammerschmidt@googlemail.com
(K.H.)

In brief

Tang et al. report a facultative life cycle of a unicellular cyanobacterium in which multicellular filaments alternate with unicellular stages depending on salinity and population density. Filament fragmentation is likely mediated in a nonlinear way by compounds in the medium and occurs through connection cleavage rather than cell death.

CellPress

Report

An environmentally induced multicellular life cycle of a unicellular cyanobacterium

Si Tang,[1,3,5] Yuriy Pichugin,[2,4,5,*] and Katrin Hammerschmidt[1,6,*]
[1]Institute of General Microbiology, Kiel University, Kiel, Germany
[2]Department of Evolutionary Theory, Max Planck Institute for Evolutionary Biology, Plön, Germany
[3]Present address: Shenzhen Public Platform for Screening and Application of Marine Microbial Resources, Shenzhen International Graduate School, Tsinghua University, Shenzhen 518055, Guangdong Province, PR China
[4]Present address: Department of Ecology and Evolutionary Biology, Princeton University, Princeton, NJ, USA
[5]These authors contributed equally
[6]Lead contact
*Correspondence: pichugin@princeton.edu (Y.P.), katrinhammerschmidt@googlemail.com (K.H.)
https://doi.org/10.1016/j.cub.2023.01.069

SUMMARY

Understanding the evolutionary transition to multicellularity is a key problem in biology.[1–4] Nevertheless, the ecological conditions driving such transitions are not well understood. The first known transition to multicellularity occurred 2.5 billion years ago in cyanobacteria,[5–7] and today's cyanobacteria are characterized by enormous morphological diversity. They range from unicellular species; unicellular cyanobacteria with packet-like phenotypes, e.g., tetrads; and simple filamentous species to highly differentiated filamentous species.[8–10] The cyanobacterium *Cyanothece* sp. ATCC 51142, an isolate from the intertidal zone of the U.S. Gulf Coast,[11] was classified as a unicellular species.[12] We report a facultative life cycle of *Cyanothece* sp. in which multicellular filaments alternate with unicellular stages. In a series of experiments, we identified salinity and population density as environmental factors triggering the phenotypic switch between the two morphologies. Then, we used numerical models to test hypotheses regarding the nature of the environmental cues and the mechanisms underlying filament dissolution. While the results predict that the observed response is likely caused by an excreted compound in the medium, we cannot fully exclude changes in nutrient availability (as in Tuomi et al.[13] and Matz and Jürgens[14]). The best-fit modeling results show a nonlinear effect of the compound, which is characteristic of density-dependent sensing systems.[15,16] Furthermore, filament fragmentation is predicted to occur by connection cleavage rather than cell death of each alternating cell, which is supported by fluorescent and scanning electron microscopy results. The switch between unicellular and multicellular morphology constitutes an environmentally dependent life cycle that is likely an important step en route to permanent multicellularity.

RESULTS AND DISCUSSION

The filamentous morphology depends on the environment

To investigate the environmental factors that favor a multicellular morphology, we exposed the unicellular cyanobacterium *Cyanothece* sp. ATCC 51142 (hereafter *Cyanothece* sp.) to the range of salinities comparable to conditions in its native habitat, the intertidal zone of the U.S. Gulf Coast.[11] When culturing replicate populations of *Cyanothece* sp. in media with different amounts of added NaCl (0–300 mM), we observed two distinct microbial lifestyles: the previously described unicellular stage[11] and a newly observed filamentous stage (Figure 1A). The occurrence of filaments depended on the salinity of the medium: at 0 mM NaCl, the entire population exhibited a filamentous morphology, ranging from 4-cell to 16-cell filaments, while at 300 mM NaCl (30 PSU), the entire population was unicellular. At intermediate salinities, we always observed both types—4-cell filaments and single cells—with a higher fraction of filaments up to

90 mM NaCl, while at higher salinities single cells were the predominant morphology. Based on the repeatability between populations and the high frequency of the filamentous stage within populations, genetic changes such as mutation or gene amplification[17] can be excluded as the cause for the change in morphology. Furthermore, the co-existence of both morphological stages in the intermediate salinities indicates phenotypic heterogeneity.

Phenotypic heterogeneity is known for many bacteria and is defined as diverse phenotypes arising from genetically identical microbes residing in the same microenvironment.[18] Several molecular mechanisms underpin phenotypic heterogeneity, such as stochastic state switching, periodic oscillations, cellular age, and cell-to-cell interactions. While in this study stochastic state switching can be excluded due to the exclusivity of one of the two stages in the two extreme environments (0 and 300 mM NaCl), periodic oscillations and cellular age can be excluded when comparing the populations in the different salinities, as all populations were initiated from the same culture. This
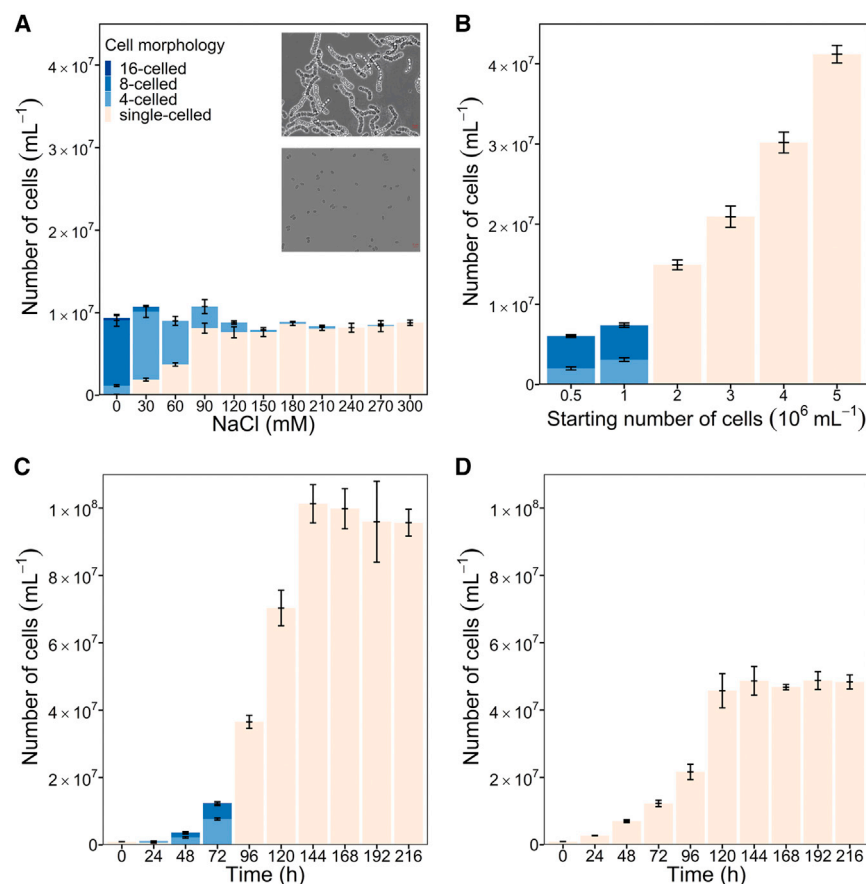
Figure 1. Cell morphologies in *Cyanothece* sp. populations as a function of salinity and population density

(A) The filamentous morphology, shown in the top inlay photomicrograph in contrast to the unicellular stage (bottom inlay), significantly depends on the salinity of the medium (ANOVA, $F_{10,32} = 953.10$, $p < 0.0001$; 0–300 mM NaCl added to BG11; populations initiated with $5*10^5$ cells/mL; measured after 48 h), and populations with a higher fraction of filaments contain higher cell numbers/mL (ANOVA, $F_{1,32} = 11.658$, $p = 0.0018$). Scale bar, 5 μm.

(B) Cell morphologies significantly depend on the starting population density ($x^2 = 16.89$, d.f. = 5, p = 0.0047; in BG11 without added NaCl; measured after 48 h).

(C) Population dynamics over the period of 9 days in BG11 *without* added NaCl (populations initiated with $5*10^5$ cells/mL).

(D) Population dynamics over the period of 9 days in BG11 *with* added NaCl (300 mM) (populations initiated with $5*10^5$ cells/mL). Transiently filamentous populations (C) grew faster and reached higher cell densities than unicellular populations (D) (ANOVA, $F_{1,5} = 331.38$, $p < 0.0001$). All experiments were performed in 10 mL medium, but note that the population composition differed depending on the volume of the medium. While the same pattern and transitions between single cells and filaments were observed in volumes of 1 mL each, filaments were present for a shorter time, such that populations contained single cells as early at 72 h post-inoculation.

Error bars represent SDs (of each sub-bar for A–C) (n = 3).

See also Figures S1 and S2.

suggests that cell-to-cell interactions are the most likely mechanism underpinning the switch between the two different phenotypes, which is confirmed by the results of the experiment investigating the effect of initial population density on lifestyle. Here, replicate populations were initiated with six different starting population densities (all from the same culture), ranging from $5*10^5$ to $5*10^6$ cells/mL (Figure 1B). We found that starting cell density was a good predictor of *Cyanothece* sp. morphology—after 48 h, the filamentous stage was only observed at lower population densities ($\leq 1 \times 10^6$ mL^{-1}), while only single cells were detected at higher densities. This suggests that an increase in cell-to-cell interactions prevents the formation of the filamentous stage. Cell-to-cell interactions could occur either by direct contact between cells[19] or indirectly, e.g., in response to cues from other cells excreted into the medium, e.g., by quorum sensing,[20] or by consumption of nutrients.

To investigate the effect of population density on population composition in more detail, we followed replicate populations inoculated with single-celled *Cyanothece* sp. of the low-density populations in NaCl-free medium for 9 days (Figure 1C). We first detected 4-cell filaments after 24 h, after which the whole population became filamentous and consisted mainly of 4- and 8-cell filaments at 48 h, and of 4-, 8-, and 16-cell filaments at 72 h post-inoculation. Thereafter, the elongation of the filaments stopped, and from 96 h post-inoculation onward, we only observed single cells. Interestingly, transiently filamentous populations grew

faster and reached higher cell densities than unicellular populations (Figures 1D and S1). Comparable life cycles with alternating unicellular and multicellular life stages have also been described for other unicellular bacteria, such as *Bacillus subtilis*, which alternate between unicellular, filamentous, and dormant life stages,[21] and for experimental populations of *Pseudomonas fluorescens*.[22]

Cyanobacterial morphology switches are mediated by external cues

The results so far suggest that the observed switches between single cells and filaments and back are density dependent—at higher cell densities, filamentation is inhibited and filament fragmentation is induced. This could be mediated by mechanisms of direct cell-cell contact or by depleted or excreted compounds in the medium. To test this, we harvested supernatants from cultures that did not produce filaments (filament inhibitor), as well as supernatants from cultures immediately after filament fragmentation (filament fragmentor).

To test whether compound (i.e., nutrient) depletion hinders filamentation, we added fresh culture medium (BG11) to both supernatants and to ddH$_2$O, creating BG11 dilutions from 0% to 100% with 20% increments. While we observed filaments at low media concentrations in ddH$_2$O (20% BG11; Table S1), we had to add more BG11 to the two supernatants (60%, 80% BG11) to observe the multicellular morphology. Since nutrient
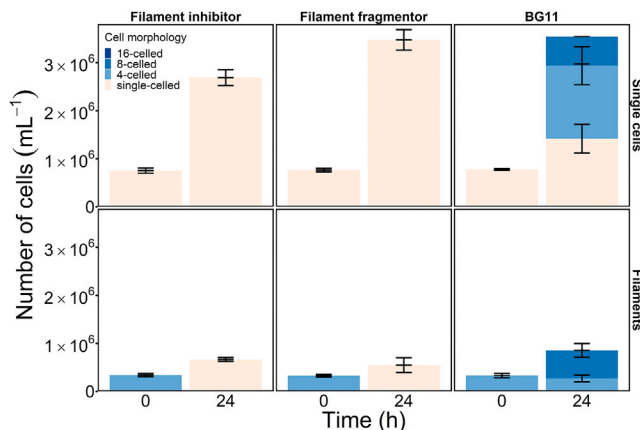
Figure 2. Cell morphology depends on the external medium
Filament inhibitor (supernatants from cultures inoculated with 5*10^6 cells/mL starting cell densities, harvested 24 h after inoculation) and filament fragmentor (supernatants from cultures inoculated with 5*10^5 cells/mL cell densities immediately after filament fragmentation, harvested at 96 h) supernatants stop the formation of filaments from single cells and lead to the dissolution of existing filaments within 24 h of exposure. This differs significantly from the control, untreated freshwater medium (BG11 without added NaCl), which induces filament formation from single cells and filament elongation (ANOVA, $F_{3,35} = 12.25$, $p < 0.0001$). Error bars represent SDs of each sub-bar (n = 3).
See also Table S1 and Figure S2.

levels are lowest in the 20% BG11:ddH$_2$O mixture, where filament formation was observed (in contrast to the 60% and 80% BG11:supernatant mixture), general nutrient depletion can be excluded as the factor hindering filamentation. This is supported by the growth trajectories of single cells after fragmentation (Figure 1C), which show that cells can still reproduce (in fact, they exhibit the shortest generation time in the period immediately after fragmentation; Figure S1) and reach a high final concentration in the media post-fragmentation, suggesting that the post-fragmentation medium (i.e. filament fragmentor) contains sufficient nutrients for growth. This is also reflected in the results of the density-dependent experiment (Figure 1B), which show cell density reaches ~4.1*10^7 cells/mL after 48 h when starting with 5*10^6 cells/mL. It should be noted that although we show that the post-fragmentation medium contains sufficient nutrients for growth, we cannot completely exclude the possibility that a particular compound required to maintain growth in the filamentous form is missing.

To test whether accumulating compounds hinder filamentation and trigger fragmentation, the harvested filament inhibitor and fragmentor supernatants were also added to cultures of low-density single cells and to 48-h-old filaments and compared to a control. After 24 h of incubation, we found that both treatments differed from the control (Figure 2). While in the control single cells formed filaments and filaments did not fragment, both supernatants inhibited filament formation from single cells and also caused filament fragmentation. This strongly suggests that the phenotypic change is not related to direct cell-cell contact, but that accumulating substances (or the depletion of specific substances) in the supernatant influence the transition between the two phenotypes. Interestingly, both supernatants

can be used interchangeably—both are able to inhibit filament formation from a unicellular ancestor and also induce filament fragmentation. However, whether or not both supernatants contain an identical substance remains to be investigated.

Since we only observed comparatively short filaments, i.e., with a maximum of 16 cells, before they disintegrated, we investigated whether this was due to culture density (mediated by substances or the absence of substances in the supernatant) or whether it was also modulated by other factors that might limit filament length. To test this, we diluted cultures containing filaments at 72 h by adding fresh culture medium. We found that filaments increase in lengths in diluted cultures (Figure S2), indicating that culture density affects filament length.

Mechanisms of filament dissolution and compound action

To learn more about the nature of the compound and the way in which filaments transition to single cells, the experimental data were fitted with a series of models to compare different hypotheses about (1) the mechanism of filament dissolution, i.e., cell death or cleavage of the connection sites, and (2) the dynamics of the compound, i.e., whether the observed pattern is caused by the accumulation or consumption of a compound. We considered three families of models. The first family, the toxic compound models (12 models; Table S2), assumes that cells produce a compound that leads to cell death and thus fragmentation of the filaments. The second family, the disconnecting compound models (12 models; Table S2), assumes that cells produce a compound that leads to the cleavage of connections between cells. The third family, the connecting compound models (8 models; Table S3), complements the previous one: these models assume that an initially present compound stabilizes the connections between cells, and its consumption causes connection loss and filament fragmentation. In each family, we consider a range of models that differ in the type of compound effect (rate of cell death or connection loss) depending on the compound concentration. These 32 models (Figure S3) account for a more diverse set of possible dynamics of environment-dependent filament fragmentation than the models previously used in theoretical studies.[23]

We found that (dis)connecting models, in which fragmentation is caused by the loss of cell connections, fit significantly better than the toxic compound models, leading to cell death (Figure 3A). Specifically, toxic compound models are unable to sustain a purely unicellular population—multicellular filaments must be present in any stable population. In particular, we show that if filament fragmentation is caused by cell death, half of the population must be filamentous (STAR Methods)—something we do not observe in the experiment. Even if we assume that the compound selectively kills every second cell in each filament, such a rapid transition from the filamentous population to a completely unicellular one, as we observed, means that the population must suffer a massive loss. However, we observe no significant change in the population growth rate at the time of filament dissolution (Figure 4A). Thus, we conclude that the observed population dynamics seem to be caused by cells disconnecting from each other rather than cell death compromising filament integrity.

This finding is supported by empirical evidence, as we did not observe cell death in the experimental cyanobacterial
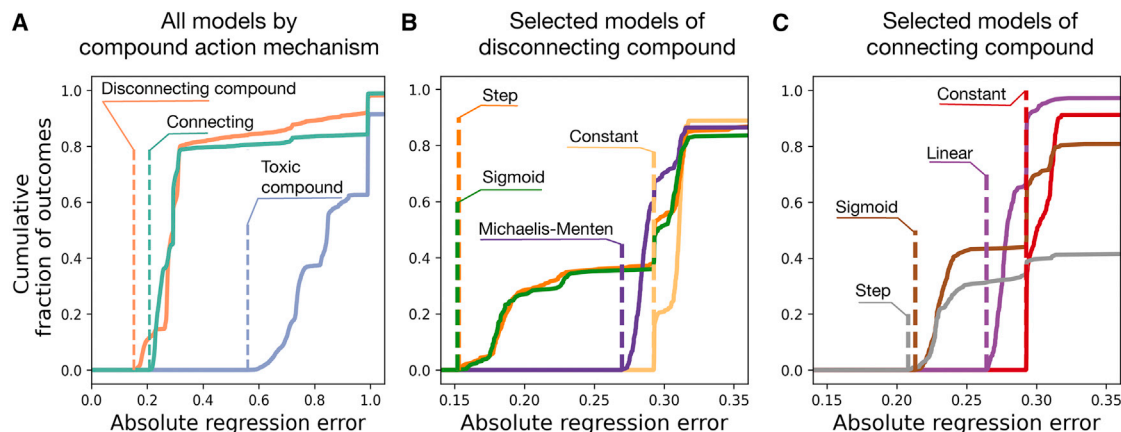
Figure 3. Theoretical prediction of mechanisms of filament dissolution and compound action

(A) Models in which connections are destroyed due to production (orange, 12 models in total) or consumption (green, 8 models) of a (dis)connecting compound provide much smaller regression errors than models with a toxic compound (blue, 12 models). (Dis)connecting models fit significantly better than the toxic compound models (one-sided Mann-Whitney U test between the regression errors of the models with toxic and disconnecting compounds, U = 739,355, n_{toxic} = 3,000, $n_{disconnecting}$ = 2,884, p < 10^{-10}, and the same level of significance was found when we contrasted the models with toxic and connecting compound models).

(B) For models with a disconnecting compound (the best class overall), the smallest regression errors were observed among models in which the rate of connection cleavage is negligible at compound concentrations below a certain threshold (e.g., in the step and sigmoid models). They thus suggest a strong non-linear response to active substance concentrations.

(C) For models with a connecting compound, the smallest regression errors were observed among models in which the rate of connection cleavage can quickly rise with the compound depletion (e.g., also in the step and sigmoid models). Only four models from each class are shown. Plots show sample cumulative distribution functions of regression errors from 250 independent optimizations for each model. Dashed lines represent the minimal regression error in each group. See also Figures S3 and S4.

populations. Using scanning electron microscopy (SEM) on 72-h-old filaments, we found that the size of the connecting areas between cells varied greatly. While some cells share a larger area with their neighboring cell, other connections are thinner and seem to disconnect easily (see example filament with breaking connection; Figure 4B). Presumably, the filaments dissolve during filament fragmentation due to breaking of these weak connections.

From a theoretical perspective, multicellular life cycles with fission into multiple pieces have a selective advantage if a fragmentation event is costly in some way.[24,25] A typical mechanism making fragmentation costly is the cell death observed in some species of filamentous cyanobacteria, where specific cells, the necridia, undergo programmed cell death when releasing hormogonia (motile reproductive filaments) from the mother filament.[26] However, the modeling results combined with the fluorescence and SEM results suggest that cell death does not happen here. The next alternative is that either the production of inhibitor/fragmentor or the response to its high concentration is costly.

Comparing the remaining models (i.e., the connecting and disconnecting families) shows that the rate of filament fragmentation must depend non-linearly on the compound concentration in order to observe the patterns found in the experiments. In all of the best-fitting models, the fragmentation rate skyrockets at a certain point in time: either after a threshold concentration of the compound is exceeded in the disconnecting compound models (in step and sigmoid models in Figure 3B and also in fracture and in breaking point models in Figure S4A) or after the compound is consumed in the connecting models (step, sigmoid, and quadratic concave in Figure 3C plus inverse and

exponent models in extended Figure S4B). Since the fitting results indicate a more complex response of *Cyanothece* sp. to inhibitor/fragmentor than the simple mass action law, this supports the hypothesis that some dedicated mechanism is involved in the observed dissolution of filaments, such as quorum sensing.

Quorum sensing is the classic example for phenotypic switching triggered by cues in the medium.[20] The known mechanisms of quorum sensing involve cell-to-cell signaling by molecules called autoinducers. They are part of a regulatory pathway with a positive feedback loop—the more autoinducer molecules present, the higher their production rate.[15,16] Consequently, the kinetic models of quorum sensing exhibit bi-stable dynamics: the cell is either on or off. While the precise kinetics and regulation of the compound are beyond the scope of this study, the known kinetic models of quorum sensing are best represented by the step model (Figure S4). An equally well-fitting sigmoid model is the generalization of the step model. These two models show the two best fits in both model families: connecting and disconnecting compound (Tables S2 and S3).

Environmentally mediated life cycles and the transition to multicellularity

This is the first report of an environment-dependent life cycle for unicellular cyanobacteria, but such life cycles are also known for other bacteria, such as *Bacillus subtilis*, which similarly switches between motile unicellular and filamentous stages.[21] Transitions from unicellular to multicellular stages in response to environmental cues also occur in slime molds,[27] choanoflagellates,[28] and even animals.[29] Furthermore, theoretical models of life cycle
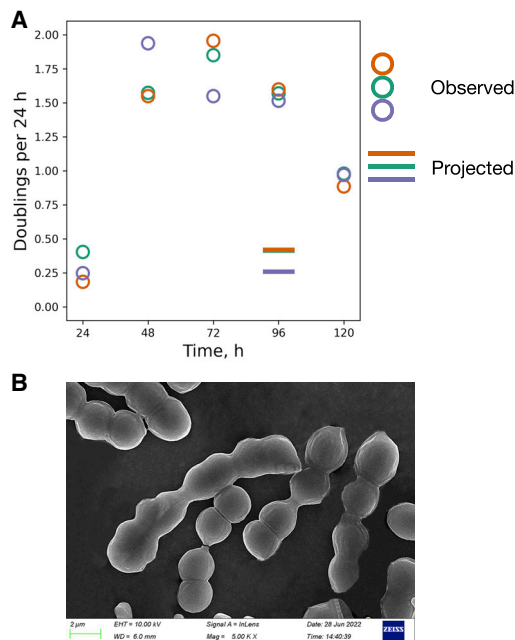
Figure 4. Filaments dissolve by fragmentation

(A) The growth rates of the replicate cyanobacterial populations as a function of time show that the population growth rate does not change at the time of filament dissolution. The colored circles are data from experimental replicates (n = 3; the value plotted at X h is the number of cell doublings between X–24 and X h). The colored lines at 96 h (the timepoint at which the filaments have dissolved into single cells) show what the population growth rate would be if every second cell in a filament died and the remaining cells were released as single cells. These predicted values are much lower than those actually observed. The fragmentation was therefore not caused by death of cells.

(B) Scanning electron photomicrographs of 72-h-old filaments of *Cyanothece* sp. Note the breaking cell-cell connection in the center filament. The tightly connected cells are probably cells that are undergoing (or have completed) cell division, and the cells with weaker connections have likely undergone cell division in earlier rounds. Scale bar, 2 μm.

evolution have shown that a changing environment can indeed lead to the evolution of life cycles with alternating unicellular and multicellular stages.[30]

Within the cyanobacteria, our observation seems to be most similar to the cyanobacteria traditionally assigned to section II (unicellular and organized into packet-like structures[10]). While it has long been known that these species rarely occur as single cells, but mostly as micro- or macroscopic, irregular, formless, or granular colonies,[31] it has recently been reported that a species belonging to this group also shows morphological phenotypic plasticity—alternating between single cells, dyads (2-celled colonies), triads (3-celled colonies), tetrads (4-celled colonies), and colonies with more than four cells—depending on the chemical composition of the culture medium and its growth stage.[32] While in our case we also observe morphological phenotypic plasticity depending on the environment, we see the formation of filaments (the underlying morphology within the cyanobacterial sections with complex multicellularity) in a classically described unicellular cyanobacterium.[10,11]

Although this facultative life cycle was artificially induced in the laboratory, it seems to be realistic for what could happen in

nature. The repeated filamentation and fragmentation in *Cyanothece* sp. could be the core of an environmentally dependent life cycle. Such a hypothetical life cycle would start as soon as single cells are in a compartment with reduced salinity, e.g., in an estuary. There, filaments would form until high local densities are reached. Overcrowding would lead to fragmentation of the filaments into independent cells. Given the small size of single cells compared to multicellular filaments, it is much more likely that the newly released single cells would be moved away from the crowded environment—either into the sea or into another fresh-water compartment, where the cycle starts again.

Importantly, many habitats are characterized by rapidly changing environmental conditions, so that, for example, a unicellular organism isolated in one environment may have a completely different phenotype/life stage in another. While it is tempting to classify organisms based on their phenotype, it is important to realize that in the laboratory we often study only parts of an organism's life cycle. This is particularly relevant for the field studying the transition to multicellularity, where the importance of phenotypic plasticity driving ancestral life cycles and providing the base for later integration, i.e., endogenization of life cycles, is becoming increasingly apparent.[30,33–36]

STAR★METHODS

Detailed methods are provided in the online version of this paper and include the following:

- KEY RESOURCES TABLE
- RESOURCE AVAILABILITY
  - Lead contact
  - Materials availability
  - Data and code availability
- EXPERIMENTAL MODEL AND SUBJECT DETAILS
  - *Cyanothece* sp. stocks
- METHOD DETAILS
  - Effects of salinity and population density
  - Supernatant test
  - Scanning election microscopy (SEM)
- QUANTIFICATION AND STATISTICAL ANALYSIS
  - Quantification of population density and composition
  - Statistical analysis
  - Theoretical model
  - Data fitting and regression results
  - Half of the stationary population, where filaments disintegrate due to cell death must be filamentous
  - Comparison of our study to the cyanobacterial filament fragmentation model by Rossetti et al. (2011)

SUPPLEMENTAL INFORMATION

Supplemental information can be found online at https://doi.org/10.1016/j.cub.2023.01.069.

REFERENCES

1. Maynard Smith, J., and Szathmáry, E. (1997). The Major Transitions in Evolution (Oxford University Press).

2. Szathmáry, E. (2015). Toward major evolutionary transitions theory 2.0. Proc. Natl. Acad. Sci. USA *112*, 10104–10111.

3. Herron, M.D., Conlin, P.L., and Ratcliff, W.C. (2022). The Evolution of Multicellularity (CRC Press).

4. Bonner, J.T. (1998). The origins of multicellularity. Integr. Biol. *1*, 27–36.

5. Schopf, J.W. (1993). Microfossils of the Early Archean Apex chert: new evidence of the antiquity of life. Science *260*, 640–646.

6. Grosberg, R.K., and Strathmann, R.R. (2007). The evolution of multicellularity: a minor major transition? Annu. Rev. Ecol. Evol. Syst. *38*, 621–654.

7. Knoll, A.H. (2015). Life on a Young Planet: The First Three Billion Years of Evolution on Earth-Updated Edition (Princeton University Press).

8. Claessen, D., Rozen, D.E., Kuipers, O.P., Søgaard-Andersen, L., and Van Wezel, G.P. (2014). Bacterial solutions to multicellularity: a tale of biofilms, filaments and fruiting bodies. Nat. Rev. Microbiol. *12*, 115–124.

9. Herrero, A., Stavans, J., and Flores, E. (2016). The multicellular nature of filamentous heterocyst- forming cyanobacteria. FEMS Microbiol. Rev. *40*, 831–854.

10. Rippka, R., Deruelles, J., Waterbury, J.B., Herdman, M., and Stanier, R.Y. (1979). Generic assignments, strain histories and properties of pure cultures of cyanobacteria. Microbiology *111*, 1–61.

11. Reddy, K.J., Haskell, J.B., Sherman, D.M., and Sherman, L.A. (1993). Unicellular, aerobic nitrogen-fixing cyanobacteria of the genus *Cyanothece*. J. Bacteriol. *175*, 1284–1292.

12. Sánchez-Baracaldo, P. (2015). Origin of marine planktonic cyanobacteria. Sci. Rep. *5*, 1–10.

13. Tuomi, P., Fagerbakke, K.M., Bratbak, G., and Heldal, M. (1995). Nutritional enrichment of a microbial community: the effects on activity, elemental composition, community structure and virus production. FEMS Microbiol. Ecol. *16*, 123–134.

14. Matz, C., and Jürgens, K. (2003). Interaction of nutrient limitation and protozoan grazing determines the phenotypic structure of a bacterial community. Microb. Ecol. *45*, 384–398.

15. Dockery, J.D., and Keener, J.P. (2001). A mathematical model for quorum sensing in *Pseudomonas aeruginosa*. Bull. Math. Biol. *63*, 95–116.

16. Chopp, D.L., Kirisits, M.J., Moran, B., and Parsek, M.R. (2002). A mathematical model of quorum sensing in a growing bacterial biofilm. J. Ind. Microbiol. Biotechnol. *29*, 339–346.

17. Darmon, E., and Leach, D.R.F. (2014). Bacterial genome instability. Microbiol. Mol. Biol. Rev. *78*, 1–39.

18. Ackermann, M. (2015). A functional perspective on phenotypic heterogeneity in microorganisms. Nat. Rev. Microbiol. *13*, 497–508.

19. Blango, M.G., and Mulvey, M.A. (2009). Bacterial landlines: contact-dependent signaling in bacterial populations. Curr. Opin. Microbiol. *12*, 177–181.

20. Waters, C.M., and Bassler, B.L. (2005). Quorum sensing: cell-to-cell communication in bacteria. Annu. Rev. Cell Dev. Biol. *21*, 319–346.

21. van Gestel, J., Ackermann, M., and Wagner, A. (2019). Microbial life cycles link global modularity in regulation to mosaic evolution. Nat. Ecol. Evol. *3*, 1184–1196.

22. Hammerschmidt, K., Rose, C.J., Kerr, B., and Rainey, P.B. (2014). Life cycles, fitness decoupling and the evolution of multicellularity. Nature *515*, 75–79.

23. Rossetti, V., Filippini, M., Svercel, M., Barbour, A.D., and Bagheri, H.C. (2011). Emergent multicellular life cycles in filamentous bacteria owing to density-dependent population dynamics. J. R. Soc. Interface *8*, 1772–1784.

24. Pichugin, Y., Peña, J., Rainey, P.B., and Traulsen, A. (2017). Fragmentation modes and the evolution of life cycles. PLoS Comput. Biol. *13*, e1005860.

25. Pichugin, Y., and Traulsen, A. (2020). Evolution of multicellular life cycles under costly fragmentation. PLoS Comput. Biol. *16*, e1008406.

26. Nürnberg, D.J., Mariscal, V., Parker, J., Mastroianni, G., Flores, E., and Mullineaux, C.W. (2014). Branching and intercellular communication in the Section V cyanobacterium *Mastigocladus laminosus*, a complex multicellular prokaryote. Mol. Microbiol. *91*, 935–949.

27. Bonner, J.T. (2015). Cellular Slime Molds (Princeton University Press).

28. Fairclough, S.R., Dayel, M.J., and King, N. (2010). Multicellular development in a choanoflagellate. Curr. Biol. *20*, R875–R876.

29. Ros-Rocher, N., Pérez-Posada, A., Leger, M.M., and Ruiz-Trillo, I. (2021). The origin of animals: an ancestral reconstruction of the unicellular-to-multicellular transition. Open Biol. *11*, 200359.

30. Pichugin, Y., Park, H.J., and Traulsen, A. (2019). Evolution of simple multicellular life cycles in dynamic environments. J. R. Soc. Interface *16*, 20190054.

31. Komárek, J. (1993). Validation of the genera *Gloeocapsopsis* and *Asterocapsa* (Cyanoprocaryota) with regard to species from Japan, Mexico and Himalayas. Bull. Natl. Sci. Mus. Tokyo Ser. B Bot. *19*, 19–37.

32. Urrejola, C., von Dassow, P., van den Engh, G., Salas, L., Mullineaux, C.W., Vicuña, R., and Sánchez-Baracaldo, P. (2020). Loss of filamentous multicellularity in cyanobacteria: the extremophile *Gloeocapsopsis* sp. strain UTEX B3054 retained multicellular features at the genomic and behavioral levels. J. Bacteriol. *202*, e00514–e00519.

33. Brunet, T., and King, N. (2017). The origin of animal multicellularity and cell differentiation. Dev. Cell *43*, 124–140.

34. Staps, M., van Gestel, J., and Tarnita, C.E. (2019). Emergence of diverse life cycles and life histories at the origin of multicellularity. Nat. Ecol. Evol. *3*, 1197–1205.

35. Bourrat, P., Doulcier, G., Rose, C.J., Rainey, P.B., and Hammerschmidt, K. (2022). Tradeoff breaking as a model of evolutionary transitions in individuality and limits of the fitness-decoupling metaphor. eLife *11*, e73715. https://doi.org/10.7554/eLife.73715.

36. Rose, C.J., and Hammerschmidt, K. (2021). What do we mean by multicellularity? The Evolutionary Transitions Framework provides answers. Front. Ecol. Evol. *9*, 730714. https://doi.org/10.3389/fevo.2021.730714.

37. Schindelin, J., Arganda-Carreras, I., Frise, E., Kaynig, V., Longair, M., Pietzsch, T., Preibisch, S., Rueden, C., Saalfeld, S., Schmid, B., et al. (2012). Fiji: an open-source platform for biological-image analysis. Nat. Methods *9*, 676–682.

38. Mareš, J., Johansen, J.R., Hauer, T., Zima, J., Jr., Ventura, S., Cuzman, O., Tiribilli, B., and Kaštovský, J. (2019). Taxonomic resolution of the genus *Cyanothece* (Chroococcales, Cyanobacteria), with a treatment on *Gloeothece* and three new genera, *Crocosphaera, Rippkaea,* and *Zehria*. J. Phycol. *55*, 578–610.

STAR★METHODS

KEY RESOURCES TABLE

REAGENT or RESOURCE	SOURCE	IDENTIFIER
Bacterial and virus strains		
Cyanothece sp.	ATCC	ATCC 51142
Chemicals, peptides, and recombinant proteins		
NaCl	ROTH	9625.1; CAS: 7647-14-5
Deposited data		
Data	This paper	https://doi.org/10.5281/zenodo.7491536
Code and simulation results	This paper	https://doi.org/10.5281/zenodo.7373857
Software and algorithms		
ImageJ	Schindelin et al.[37]	https://imagej.nih.gov/ij/
Other		
ASP2 Medium	Reddy et al.[11]	N/A
BG11 Medium	Rippka et al.[10]	N/A

RESOURCE AVAILABILITY

Lead contact
Further information and requests for information should be directed to and will be fulfilled by the lead contact, Katrin Hammerschmidt (katrinhammerschmidt@googlemail.com).

Materials availability
This study did not generate new unique reagents, organisms or materials. *Cyanothece* sp. ATCC 51142 can be obtained from the American Type Culture Collection (ATCC).

Data and code availability

- All data reported in this paper has been deposited in a Zenodo repository and is publicly available as of the date of publication (https://doi.org/10.5281/zenodo.7491536).
- All original code has been deposited in a Zenodo repository and is publicly available as of the date of publication (https://doi.org/10.5281/zenodo.7373857).
- Any additional information required to reanalyze the data reported in this paper is available from the lead contact upon request.

EXPERIMENTAL MODEL AND SUBJECT DETAILS

Cyanothece sp. stocks
Cyanothece sp. ATCC 51142 (recently reclassified as *Crocosphaera subtropica*[38]) was obtained from the ATCC culture collection. Stock cells were grown photoautotrophically at continuous light with a light intensity of 30 μmol m^{-2} s^{-1} in liquid culture (artificial seawater medium ASP2[11]) at 30°C.

METHOD DETAILS

Effects of salinity and population density
To evaluate the effect of salinity on the morphology of *Cyanothece* sp., we performed a growth experiment (starting with $5*10^5$ cells/mL), in which we supplemented BG11 medium[10] with NaCl. In total, we tested three replicates in each of the eleven NaCl concentrations (0, 30, 60, 90, 120, 150, 180, 210, 240, 270, 300 mM) with a total volume of 10 mL. We recorded the population composition 48 h after the start of the experiment. To test for the effect of starting population density on the morphology of *Cyanothece* sp., we created a gradual series of starting population densities ($5*10^5$, 10^6, $2*10^6$, $3*10^6$, $4*10^6$, $5*10^6$ cells/mL, a total volume of 10 mL), with three replicates per condition. We again recorded the population composition 48 h after the start of the experiment.

Supernatant test

To test whether the phenotypic switch is mediated by nutrient depletion, fresh culture medium (BG11) was diluted with filament inhibitor, filament fragmentor and ddH$_2$O, creating a gradual series of BG11 ratios (0 %, 20 %, 40 %, 60 %, 80 %, 100 %), within a total volume of 1 mL. Low-density single cells (5*10^5 cells/mL) were cultured in all combinations in the 24-well plate, with three replicates for each combination. After 48 h, the morphology of the cells within each replicate was observed under the microscope and the presence of filaments was recorded.

To investigate whether filament fragmentation depends on cellular age, single cells were grown in 10 mL BG11 in tissue culture flasks for 72 h, after which filament formation was confirmed under the microscope. Cultures were gently mixed, and 20 μL of the filamentous *Cyanothece* sp. population was transferred to 980 μL of fresh BG11 medium. As a control, 1 mL of culture without the addition of fresh medium was grown in parallel. Each treatment was carried out with three replicates. After 24 h, replicate populations (n = 3 each) were quantified.

To differentiate whether the morphology changes from single cells to filaments and back have been induced by direct cell-cell contact or through (excreted) compounds in the media, we harvested two supernatants: (i) filament inhibitor, and (ii) filament fragmentor. We created the filament inhibitor supernatant by setting up replicate cultures (n = 3) with high starting cell densities (5*10^6 cells/mL) in BG11 media. We let them grow for 24 h under the conditions described above, after which we centrifuged samples (at 20 × g for 3 min). Thereafter we processed the supernatant through a 0.22 μm filter (Syringe filter, membrane: PES) to exclude cyanobacterial cells. The process for harvesting the filament fragmentor supernatant was the same, only that the culture was initiated differently. Here, low-density cultures (5*10^5 cells/mL) (n = 3) were set up in BG11 and closely monitored. We harvested the supernatant directly after filament fragmentation occurred. Directly after harvesting the supernatants, we set up an experiment, where we exposed replicate populations (n = 3 each) of single cells (5*10^5 cells/mL) and 48-hours-old filaments to either filament inhibitor or filament fragmentor supernatants or to fresh BG11 media. To achieve this, 1 mL unicellular culture (exponential phase) or 1 mL of 48-hours-old filaments were centrifuged, and the resultant supernatants were discarded. Thereafter cells were resuspended in 1 mL of either filament fragmentor supernatant, filament inhibitor supernatant, or fresh BG11, respectively. We recorded the population composition 24 h after the start of the experiment.

Scanning election microscopy (SEM)

Single cells were grown in BG11 for 72 h, after which filaments were harvested by centrifugation, washed twice and resuspended in sterile PBS. Then samples were lyophilized for 12 h prior to imaging. The dried filaments were sputter-coated with a gold/palladium thin film for 100 s and a 15 mA current, using a Q150R sputter coater (Quorumtech, UK). Samples were imaged with a field-emission SEM and 10 kV electron beam (Zeiss Sigma 300, Zeiss, Germany).

QUANTIFICATION AND STATISTICAL ANALYSIS

Quantification of population density and composition

Population density and composition was quantified with a cell counting chamber (Neubauer improved, depth: 0.1 mm) from which digital photographs were taken (camera AxioCam MRR3 mounted to the microscope ZEISS Imager.M2m). More specifically, from each replicate population (total volume of 1mL) 1 μL was assayed, and cells within the final volume were calculated with the formula: Cells in 1μl = (number of cells in the main square) (1μl) /0.004. Images were counted manually using the software ImageJ, and classified into four categories: single cells, 4-celled filaments, 8-celled filaments and 16-celled filaments. In addition, we screened the populations for cell death using fluorescent microscopy (dead cyanobacterial cells can be identified by the lack of a fluorescent signal).

Statistical analysis

Statistical details for each experiment can be found in the figure legends and corresponding texts. For all experiments, 3 biological replicates were analyzed. Every measured data point, as well as the mean and SD of the 3 replicates are shown in the graphs.

Sample size was chosen to maximise statistical power and ensure sufficient replication. Assumptions of the tests, that is, normality and equal distribution of variances, were visually evaluated. Non-significant interactions were removed from the models. All tests were two-tailed. Effects were considered significant at the level of $P < 0.05$. All statistical analyses were performed with JMP 9. Graphs were produced with R Studio Version 1.4.1564 and Python Matplotlib library.

Theoretical model

In the model, we consider a population composed of filaments of different length. After division, cells always stay together, increasing the length of the filament. Cell divisions in each filament occur synchronously, so the filament length doubles at each division event. However, filaments divide independently from each other, hence division events among different filaments are not synchronized. The rate of cell division in density dependent – the more cells are present in the population, the slower is cell division:

$$W_{\text{eff}}(\mathbf{x}) = W_0 \left(1 - \frac{\sum_i i x_i}{K} \right), \qquad \text{(Equation 1)}$$

where $W_{eff}(\mathbf{x})$ is the division rate of cells in the population $\mathbf{x}$, W_0 is the maximal division rate, x_i is the number of filaments of the length i, and hence, $\sum_i ix_i$ is the total number of cells in the population, K is the maximal number of cells that can be sustained in the population (carrying capacity). The maximal possible length of the filament in the model was limited to 32 cells, which is larger than any empirically observed filament. Filaments that reach that maximal size stop dividing.

We assume that filaments fragment due to the changes in the environment caused by the presence of cells. Here we consider three families of models. In toxic compound models cells produce a compound causing cell death. In disconnecting compound models cells produce a compound causing connections cleavage. In connecting compound models cells consume a compound that underlies filamentation. In both disconnecting and connecting models, the fragmentation occurs via loss of cell connections but in the first case cells produce the mediating compound, while in the second case they consume it.

In the disconnecting and toxic compound models, cells produce a compound T, which causes filament fragmentation. Each cell produces the compound with the unit rate. Produced compound decays with the rate D_{comp}. Hence, the compound dynamics is given by

$$\frac{dT}{dt} = \sum_i ix_i - D_{comp}T, \qquad \text{(Equation 2)}$$

where the first term describes the production of compound by cells, and the second term describes the compound decay. The rate of compound production is set to one without loss of generality, as it is just a scaling factor for non-observed compound concentration.

In the connecting compound models, a fresh media initially contains a unit concentration of a compound, while cells consume the compound. Hence, the compound dynamics are governed by a different law

$$\frac{dT}{dt} = -D_{cons}T\sum_i ix_i, \qquad \text{(Equation 3)}$$

where D_{cons} is the rate at which a single cell consumes the compound.

In all cases, population dynamics are described by the set of differential equations

$$\frac{dx_i}{dt} = \sum_j A_{ij}(\mathbf{x}, T)x_j, \qquad \text{(Equation 4)}$$

where the projection matrix $A_{ij}(\mathbf{x}, T)$ shows the rate at which filaments of length i emerge from the filaments of length j by means of growth and fragmentation.

For the connecting and disconnecting compound models, filaments fragment by loosing connections between cells. Hence, the elements of this matrix are

$$A_{ij}(\mathbf{x}, T) = \begin{cases} -W_{eff}(\mathbf{x}) - (i-1)E(T), & \text{if } i = j \\ W_{eff}(\mathbf{x}), & \text{if } i = 2j \\ 2E(T), & \text{if } i < j \\ 0, & \text{otherwise} \end{cases} \qquad \text{(Equation 5)}$$

There, the first line describes the disappearance of filaments due to the growth or fragmentation, the second line describes the emergence of twice-longer filaments at each growth event, and the third line describes the emergence of shorter filaments after fragmentation. $E(T)$ is the rate of effect of compound at the concentration T. In the disconnecting compound models, $E(T)$ is a monotonically increasing function – more compound leads to higher rate of connections loss. In the connecting compound models, $E(T)$ is a monotonically decreasing function – fewer compound leads to less stable connections.

For toxic compound models, filaments fragment whenever an internal cell dies. Hence, the elements of this matrix are

$$A_{ij}(\mathbf{x}, T) = \begin{cases} -W_{eff}(\mathbf{x}) - iE(T), & \text{if } i = j \\ W_{eff}(\mathbf{x}), & \text{if } i = 2j \\ 2E(T), & \text{if } i < j \\ 0, & \text{otherwise} \end{cases} \qquad \text{(Equation 6)}$$

Note that the only difference between Equations 5 and 6 is the coefficient before $E(T)$ in the first line. This represents that in a filament of i cells, there is $i-1$ connections, which can be severed (if the fragmentation is due to the cleavage of connections) but i cells that can die (if the fragmentation is due to the death of cells).

For each family, we consider a number of models of the compound effect $E(T)$, see Figures S3 and S4 and Tables S2 and S3. There are 32 models in total. In each family, two control models represent situations, where the mechanism of the compound action is straightforward: the proportional model assumes a mass action law of the interaction between the compound and cells, the constant model assumes a spontaneous fragmentation of filaments, i.e. the compound plays no role. Other models represent situations, where the compound acts on filaments in a more complicated way.

Data fitting and regression results

Four series of experiments are taken into account in the simulations. The first data set is the population composition at different starting densities (Figure 1B). The second data set is the population composition over time (Figure 1C). The third data set is the filament elongation test (Figure S2). The fourth data set is the investigation of the supernatant effects (Figure 2). For each tested combination of parameters, the simulations imitating experimental protocols were conducted.

To simulate the experiment shown in Figure 1B, the population was initialized with solitary cells at given concentrations and the population composition after 48 h recorded for comparison with experimental observations. To simulate the experiment shown on Figure 1C, the population was initialized with solitary cells at the given concentration and the population compositions at time points 24, 48, 72, 96, and 120 h after initialization were recorded. To simulate the experiment shown on Figure 2, first, the population was initialized with high density (filamentation inhibitor), or low density (fragmentation inducer) of solitary cells, and simulated for 24 or 72 h, respectively. Then, the concentration of the compound was sampled and used in the second simulation series, initialized with populations, given by records at 0 h in each of the sub-experiments. In each case, the composition after 24 h was recorded. To simulate the experiment shown in Figure S2, the population was initialized with the experimental record given for 0 h and the population state after 48 h was recorded.

In each simulation, the mean square deviation between the experimentally observed and numerically simulated population composition was computed. Minimization of this value by adjusting growth and fragmentation parameters was the target of the fitting.

The experimental data has been fitted with each of 32 numerical models (see Tables S2 and S3 for definitions). The initial values of model parameters have been drawn randomly, so different runs of optimization ended at different points in the parameters space. To compensate for that, 250 independent optimization runs were computed for each model.

Regression errors were scaled by the error provided by the static population. This means that the fitting error provided by the population, which neither grows nor dies and is not affected by the compound, is equal to one. The hypothesis of a static scenario is clearly incorrect; therefore all fitting results with regression errors above one were discarded from the further analysis as completely unrealistic.

All toxic compound models demonstrated much larger regression errors than (dis-) connecting compound models (Figure 3A; Table S2). Among disconnecting models, four models demonstrated similar and low minimal regression errors (0.15–0.17): step, sigmoid, fracture, and breaking point. Quadratic model has shown the minimal error around 0.217. The remaining seven models (constant, proportional, linear, top-capped, bottom-capped, Michaelis-Menten, and saturating exponent) resulted in larger errors (0.26–0.29), see Figure S4 and Table S2. Among connecting compound models, the lowest regression errors (0.20–0.22) were observed for models capable to demonstrate a sudden increase in fragmentation rate at low compound concentrations (step, sigmoid, exponent, inverse, quadratic concave). At the same time, models in which the fragmentation rate increased gradually with compound loss (constant, linear, quadratic convex) resulted in larger regression errors (0.23–0.30), see Figure S4 and Table S3.

Half of the stationary population, where filaments disintegrate due to cell death must be filamentous

The toxic compound models assume that a filament breaks because a cell in it dies and can no longer hold the two side branches together. These events occur more frequently at higher concentrations of the compound – so the filaments that make up the population become shorter as the compound concentration increases in the environment. However, this process cannot bring a population to a state where only single cells exist – the observation we have made in all our experiments. This is because the concentration of the toxic compound cannot be arbitrarily high – too much compound would lead to a population decline. The maximum possible concentration of the compound (and the shortest possible filaments) is reached at the equilibrium between growth and death, when the growth of the population due to cell division is compensated for by the loss of cells through the action of the toxic compound.

Consider this equilibrium in detail, with a particular focus on solitary cells. Solitary cells arise in the population through the fragmentation of filaments after the death of a cell. There are also two processes by which solitary cells are removed from the population: Cell death due to exposure to the toxic compound and cell division, which turns a single cell into a two-celled filament. In the stationary state, the rates of gain and loss of solitary cells are equal

$$R_{gain} = R_{death} + R_{division}, \qquad \text{(Equation 7)}$$

where R_{gain} is the rate of gain of solitary cells, R_{death} is the total death rate of solitary cells, and $R_{division}$ is the total division rate of all solitary cells (all rates are per population, not per cell). Next, we elaborate on these rates. Let us denote the number of solitary cells in a population as N_1 and the number of filaments as N_F. If the division rate for a single cell is r, then the total division rate for all solitary cells is

$$R_{division} = r N_1. \qquad \text{(Equation 8)}$$

The stationary state of the population is defined by the equilibrium between cell growth (both solitary cells and filaments) and cell death, i.e. for each cell the rates of death and division are equal. Therefore, in this state, the rate of cell death is also r, so that the total rate of death among the solitary cells is

$$R_{death} = r N_1. \qquad \text{(Equation 9)}$$

Finally, the gain of solitary cells is determined by the fragmentation of filaments. There might be filaments of various lengths in the population. However, for a filament of any length, there are only two cells, which deaths release a solitary cell, i.e. the second cell at each tip. Therefore, the rate of gain is

$$R_{gain} = 2r\,N_F. \tag{Equation 10}$$

Combining Equations 7, 8, 9, and 10, we get

$$2r\,N_F = r\,N_1 + r\,N_1, \tag{Equation 11}$$

From here, it immediately follows that

$$N_F = N_1, \tag{Equation 12}$$

i.e. the number of filaments in the stationary state is equal to the number of solitary cells. This proves that the fragmentation of the filaments caused by the toxic compound cannot lead to a stable population consisting of only solitary cells, as we observe in our experiments.

Comparison of our study to the cyanobacterial filament fragmentation model by Rossetti et al. (2011)

A model of filament fragmentation has been also described by Rossetti and coworkers.[23] Their model can be considered as a specific limited case of our set of models. Both our and Rossetti et al. models examine growing populations of linear filaments and share the same logistic dependence of the cell division rate from the cell density. However, the model of Rossetti et al. includes only filament fragmentation due to cell death, while our model set also includes the mechanism of connection loss.

Another difference between the models is that in our case, cell death is caused by the compound produced by cells; while in the model of Rossetti et al. the rate of cell death depends on cell density. In both cases, more cells in a population results in a larger death rate but the model presented here features a reactivity: a sudden increase in cell count does not cause an immediate increase in death rate; instead the death rate will steadily rise with the accumulation of the compound. This difference is of principal importance: the model of Rossetti et al. is unable to recover the results of supernatant experiments presented in Figure 2 – the media plays no role in that model and it is impossible to observe high rates of filaments fragmentation at low cell densities. Nevertheless, the design of the cell death from the model of Rossetti et al. can be formally recovered by our models set by choosing the proportional model of compound action (see Table S2 and Figure S4), plus setting both compound decay rate D_{comp}, and compound toxicity α to very large values. With a high compound decay rate, the equilibration of the compound concentration will occur rapidly, so the death rate will closely follow the cell density. Since a high decay rate also means low overall concentrations of compound, to have any significance, the toxicity must also be high. With this set up our model will behave identically to the model of Rossetti et al., however by doing so, the choice of the compound action mechanism, the model of the compound action, and even the parameter values would be far from optimal.